Simulations of the bistatic scattering using two-scale model and the unified sea spectrum

Mohamed Yassine Ayari, Ali Khenchaf and Arnaud Coatanhay

Laboratory E3I2, EA 3876, ENSIETA, 29806 Brest Cedex 9, France
Ali.Khenchaf, Arnaud.Coatanhay@ensieta.fr

Abstract. This paper deals with the simulations of scattering by the sea surface using Two-Scale Model (TSM) and the realistic unified sea spectrum in various bistatic configurations. After a brief theoretical presentation, our numerical results (scattering matrix coefficients) are compared with measured data, with a semi-empirical model (CMOD5) and with other analytical models (Small Slope Approximation) in backscattering configuration. Then, we study the influence of sea parameters (wind speed and wind direction) upon the co- and cross-polarization signature in various bistatic configurations.

Finally, we present the simulation of the signal received by an observer above the sea when a plane incident wave impinges on the ocean surface.

Keywords: t wo scale model, bistatic scattering, rough surface, ocean surface.

1 INTRODUCTION

As for naval military detection, civil coast surveillance or satellite remote sensing, radar activities in maritime environment require more and more realistic models of the electromagnetic scattering by the sea surface. In truth, the interaction between an electromagnetic wave and ocean-like rough surfaces has been extensively studied in the scientific literature. For instance, we can cite the Kirchhoff Approximation (KA) [1–3], the Small-Perturbation Method (SPM) [4–6], the Phase Perturbation technique (PP) [7–9], the Integral Equation Model (IEM) [2,3,10–14], the Small Slope Approximation (SSA) [15–18], the Université Catholique de Louvain (UCL) model [19–22] or the Two-Scale Model (TSM) [23–25].

In other respects, the description of the sea wave phenomena has led to intense research activity and many papers deal with this issue. In particular, the ocean surface modelling as a function of wind speed and direction can be found in various references [26–33]. As a matter of fact, the roughness of the sea surface is characterized by a spectrum or a slope probability density function that takes into account several physical parameters. In this paper, only Cox & Munk slope distribution [26, 27, 34], semi empirical spectrum [35] and unified spectrum [33] were considered.

As a matter of fact, the relation between the wave height spectra of the sea and the observed radar cross sections is a very classical issue in oceanic remote sensing. Since the late sixties, the work of Wright [36] illustatres the relation between the roughness of the sea and the sea clutter in L, C and X-band. A decade later, Valenzuela [37] published a review about the interaction of electromagnetic and oceanic waves. Nevertheless, until very recently, the most part of the previously published papers deal with the backscattering configurations, [38–40]. Articles considering the foward-backward configurations are far less numerous [41–43], and those dealing with others bistatic configurations remains rare [23].

The purpose of our study was to evaluate the co- and cross-polarization scattering by the ocean surface in any bistatic configuration using a TSM approach with various wind conditions (speed and direction). It is noteworthy that the analysis of the bistatic signals is a growingly important issue in remote sensing because more and more new multistatic systems (with various sources of opportunity) have been investigated for several years.

In this paper, a special focus is given to numerical results and computational simulations. Finally, to put our computations into practice, we present the simulation of the signal received by an observer above the sea when a plane incident circularly polarized wave impinges on the ocean surface. As a matter of fact, this part corresponds to a simplified model for a bistatic system (based on GPS signal) applied for remote sensing activities in a maritime environment.

2 SEA SURFACE DESCRIPTION

Usually, the sea roughness is assumed to be a non time-varying phenomenon and the sea surface is considered as an ergodic and stationary random process in which the height is denoted $z\,(x,\ y)$.

In these conditions, the spectrum and density probability models appear as the most used descriptions of the sea roughness. In addition, it is essential to stress the fact that our TSM approach involves the knwoledge of both spectrum and slope models.

2.1 Sea Slope Distribution

In the 50's, Cox and Munk [26, 27, 34] generated a reliable semi-empirical slope distribution law, based on the analysis of sun glitter photographs. A comparison with the gaussian law is given in appendix A. This probability density function given as a function of wind speed and direction was applied to our TSM approach.

2.2 Sea Surface Spectrum

Therefore the Cox and Munk probability density function stands out as the only realistic sea slope distribution, many sea spectrum have already been proposed. The Gaussian spectra based on correlation distance L and wave variance σ [10, 44, 45] are too simplistic, and have to be rejected. Hovever, more elaborated models exist and can easily be evaluated.

In any case, without loss of generality, the sea spectra are supposed to be in the form:

$$S(K,\,\phi) = M(K) f(K,\,\phi) \tag{1}$$

where $M(K)$ represents the isotropic part of the spectrum modulated by the angular function $f(K,\,\phi)$. K and ϕ are respectively the spatial wave number and the wind direction. In this paper, we will refer to two models from the literature: Semi-empirical and Unified spectrum [33, 35].

2.2.1 Semi-empirical spectrum

The semi-empirical sea spectrum is based upon Pierson et al. studies [28, 46]. This spectrum is essentially characterized by the fact that the sea wave phenemenon is explicitly split into two parts. On the one hand, capillary waves directly driven by the wind are mathematically described. On the other hand, gravity waves related to the swell are described using another mathematical expression.

Figure 1 illustrates the $M(K)$ omnidirectional elevation spectrum behavior of the sea surface with the spatial wave number for two wind speed values.

To account for the anisotropic effect due to wind direction, Pierson et al. [46] came up with the angular function $f(\phi)$. Later, Chan et al. [47] introduced a more elaborated angular function denoted $f(K,\,\phi)$.

As shown in figure 2, the angular function of the Pierson-Moskowitz model is centrosymmetric and has a peak of attenuation at the cross wind direction.

Although Pierson-Moskowitz model is far more realistic if compared with Gaussian spectra, several inconsistencies remain. More specifically, to answer the spectrum continuity property, low-frequency spectrum had to be lowered by a factor of 2.88 [35]. This concession can easily distort all applications based on this spectrum.

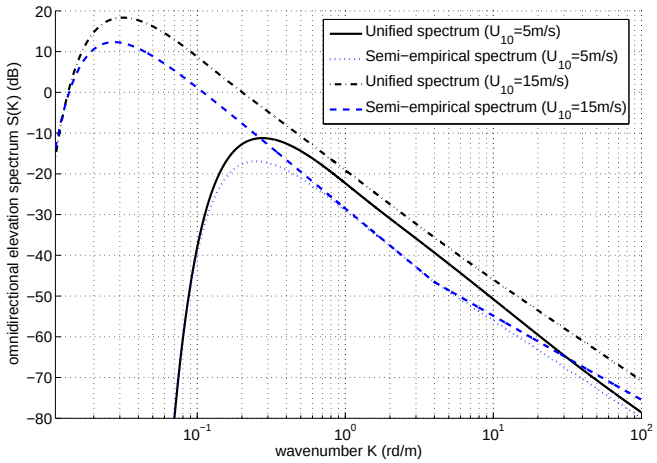

Fig. 1. Sea surface spectra: (Omnidirectional elevation spectrum)

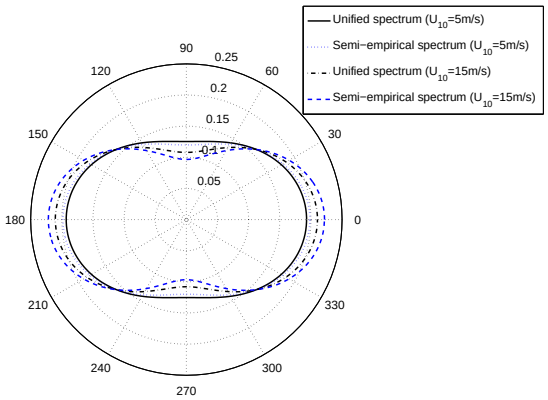

Fig. 2. Sea surface spectra: (Angular function)

2.2.2 Unified spectrum

The unified spectrum [33] was introduced by Elfouhaily et al in 1997. The purpose was to propose an improved sea spectrum that relies heavily on earlier works [35, 46, 47] but that is in better agreement with observations [26, 27, 32]. Indeed previous models are either in some parts in discordance with observations [35] or shows analytically undesirable aspects such as discontinuities across wavenumber limits, nonphysical tuning or adjustment parameters and noncentrosymmetric directional spreading function.

Based on previous spectral developments [28, 29, 31], the unified spectrum definition is much more robust since its analytic expression is available for all the wave number bands. As a matter of fact, the unified spectrum is the sum of two components (capillary and gravity waves), each of which is dominant when situated in its frequency band. Moreover, the unified spectrum takes in account the fetch influence on the wave behavior [33]. Figures 1 and 2 respectively show the fully developed isotropic unified spectrum and the unified spreading function behavior for different wind velocities. It is to be noted that the spreading function answer the centrosymmetric property as required by Guissard et al. [48].

When comparing the semi-empirical and the unified omnidirectional spectra figure-1, we

notice a difference of about 10 dB for the low wavenumbers. This can be justified by the Fung transformation to answer the Pierson-Moskowitz spectrum continuity. In a similar way, the Fung transformation involves significant differences between both spreading functions, especially for crosswind and up/downwind directions. Furthermore, these differences increase with wind speed. Finally, with sea slope distributions and sea spectra as known, the following section presents the estimation of the electromagnetic scattering by a given sea surface.

3 BISTATIC RADAR CROSS SECTION ESTIMATION

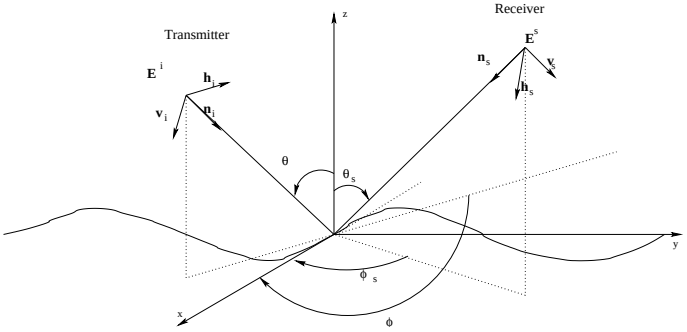

Fig. 3. geometry of the surface bistatic scattering problem

The roughness of the ocean surface induces a well-known depolarization of the electromagnetic scattered plane wave. Let $\mathbf{E}^i$ and $\mathbf{E}^s$ represent the Jones vector of the transmitted and received electromagnetic waves, respectively (see fig 3). Using an orthogonal linear (HV) polarization basis, the components of the scattered $\mathbf{E}^s$ and the incident $\mathbf{E}^i$ electric field expressed in the polarization bases ($\mathbf{v}^s$, $\mathbf{h}^s$), and ($\mathbf{v}$, $\mathbf{h}$) respectively are linearly related.

$$\begin{aligned} \mathbf{E}^s &= \begin{bmatrix} E^s_{v_s} \\ E^s_{h_s} \end{bmatrix} = \begin{bmatrix} S_{v_s v} & S_{v_s h} \\ S_{h_s v} & S_{h_s h} \end{bmatrix} \begin{bmatrix} E^i_v \\ E^i_h \end{bmatrix} \\ &= [S]\mathbf{E}^i \end{aligned} \tag{2}$$

Many approaches were developed to evaluate the electromagnetic sea surface scattering matrix. However each of them is an approximation and is based on particular assumptions and conditions.

3.1 Kirchhoff Approximation

The electromagnetic formulation of the Kirchhoff Approximation (KA) [49] is based upon the second Green theorem for vectors. It states that a scattered field at any point within the source-free region bounded by a closed surface can be expressed in terms of the tangential fields on the surface [3, 7, 9].

Once the tangential fields are determined, the scattered field can be computed. The validity conditions of the KA, due to analytic reasons, have been fully detailed in the literature [50] ($kL > 6$ and $R_c > \lambda$), where L states for the surface correlation length, and R_c is the average radius of curvature for the rough surface. Under this assumption, the analytical evaluation of the scattered field remains difficult.

To obtain a more tractable expression, two additional assumptions can be made: the scalar approximation (physical-optics PO) and the stationary phase approximation (geometric-optics GO) [7, 51, 52]. The former one is based on assuming that the rms surface slope is small,

whereas the latter approximation supposes that the variance height is larger than the incident wavelength [50, 53], and therefore this approximation determines the polarization of wave scattered for a given direction.

The contribution of the rough surface becomes identified with a plane wave reflected by an infinite plane of the same electrical properties and tangent at any of the specular points.

KA is valid for a surface with roughness scale and average curvature radius larger than the electromagnetic wavelength. In a few words, this approach is specifically used in the adopted model for the specular component determination.

When both the surface standard deviation and the correlation length become smaller than the wavelength, another standard model must be considered: the Small-Perturbation Method (SPM) [4].

3.2 Small-Perturbation Method

The Small Perturbation Method (SPM), conventionally attributed to Rayleigh [6] and continuously developed [4, 5, 7, 9], is valid for a slightly rough surface with respect to the incident wavelength. This approach applies to the cases when the phase difference due to height variation is much smaller than 2π, and the slope surface is much smaller than unity.

In practice, this approach is most of the time appropriate when the roughness of the surface can be considered as shallow with respect to the electromagnetic wavelength.

This model leads, directly from Maxwell equations and reflectivity coefficients [51, 52] to a system of six differential equations [4, 23, 50]. Using the first order of the Fourier series expansion, the differential system can be reduced to a simple six-dimensional scalar linear system [7].

Contrary to the previous model, SPM does not fit the experimental data for the specular component. On the other hand, this model is really appropriated when the scattering is situated between specular and grazing angles. It is noteworthy that for grazing scattering neither the KA nor the SPM are able to estimate the electromagnetic field.

3.3 Small Slope Approximation

The Small Slope Approximation (SSA) was proposed by Voronovich et al. [15–18] in order to reconcile SPM and KA. This approach assumes that the slopes of roughness are small compared with the angle of incidence and scattering. A noticeable characteristic of SSA is that no explicit separation between different roughness scales is required.

It clearly appears [52] that SSA has a wider validity domain than the KA and SPM approaches. Nevertheless, numerical complexity, specially when dealing with grazing angles [54, 55], constitues the main limitation of this approach. SSA involves a double integral (one space and one frequency variable) with an oscillating complex-valued kernel that exhibits branch cuts and singularities [56].

3.4 CMOD

In addition to analytical approaches, empirical models of ocean radar scattering, such as the CMOD family of C-band for European Remote Sensing Wind Scatterometer (ERS-1 and -2) , are widely used to provide quantitative information about wind fields [57]. More recently, the CMOD5 model was validated with a great number of measurements and can be considered as a reliable reference. However CMOD models are only valuable for backscattering configurations. It is also important to see that, as any empirical approach, the CMOD models do not easily lead to physical interpretations.

3.5 Two-Scale Model

In this paper, the presented simulations in bistatic configuration are mainly based on a Two-Scale Model (TSM). Generally speaking, the basic idea behind TSM approaches is to take advantage of KA and SPM in two separate validity domains.

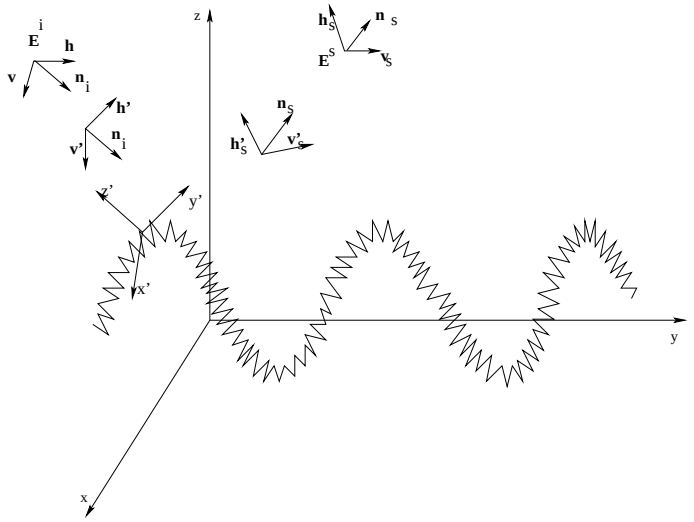

Fig. 4. Geometry of a surface bistatic scattering in the Two-Scale Model

For instance, we can cite the UCL model [19–22]. It consists of a scalar summation of the KA and SPM under appropriate conditions. In this paper, we focus in a particular TSM introduced by Fuks [58] and Fung et al. [10] in backscattering configuration and validated by Khenchaf et al. [23, 24, 50] in bistatic configurations for semi-empirical sea spectra.

In this approach, sea surface scattering is estimated in two steps. First, we focus on small scale waves using the small perturbation model, then by a tilting process we may easily determine the global component (see fig-4).

Assume the incident wave $\mathbf{E}^i$ to be

$$\mathbf{E}^i = E_0\mathbf{a} \quad \text{with} \quad E_0 = |E_0|e^{-jk\mathbf{n}_i.\mathbf{r}} \tag{3}$$

where **a** is the unit polarization vector (vertical polarization v or horizontal polarization h), k is the wave-number of the illuminating wave, and $\mathbf{n}_i$ is the unit vector in the incident direction.

In the local reference frame the incident field can be written as

$$\mathbf{E}^i = E^i_{v'}\mathbf{v}' + E^i_{h'}\mathbf{h}' = ((\mathbf{a}.\mathbf{v}')\mathbf{v}' + (\mathbf{a}.\mathbf{h}')\mathbf{h}')E_0 \tag{4}$$

and the locally scattered field due to incident waves is

$$\begin{aligned} \mathbf{E}^s &= (E^s_{v'_s}\mathbf{v}'_s + E^s_{h'_s}\mathbf{h}'_s = [S]\mathbf{E}^i \\ &= \begin{bmatrix} S_{v'_s v'}E^i_{v'} + S_{v'_s h'}E^i_{h'} \\ S_{h'_s v'}E^i_{v'} + S_{h'_s h'}E^i_{h'} \end{bmatrix} \end{aligned} \tag{5}$$

where $S_{p'q'}$ is the scattered field for unit incident fields calculated using Small Perturbation Method. Then the scattered field can be written as

$$\mathbf{E}^s = E^s_{v_s a}\mathbf{v}'_s + E^s_{h_s a}\mathbf{h}'_s = [S]\mathbf{E}^i \tag{6}$$

where the scattering matrix [S] is given by

$$
\begin{aligned}
[S] &= \begin{bmatrix} \mathbf{v}'_s \cdot \mathbf{v}_s & \mathbf{h}'_s \cdot \mathbf{v}_s \\ \mathbf{v}'_s \cdot \mathbf{h}_s & \mathbf{h}'_s \cdot \mathbf{h}_s \end{bmatrix} \\
&\quad \begin{bmatrix} S_{v'_s v'} & S_{v'_s h'} \\ S_{h'_s v'} & S_{h'_s h'} \end{bmatrix} \begin{bmatrix} \mathbf{v}' \cdot \mathbf{v} & \mathbf{v}' \cdot \mathbf{h} \\ \mathbf{h}' \cdot \mathbf{v} & \mathbf{h}' \cdot \mathbf{h} \end{bmatrix}
\end{aligned} \tag{7}
$$

For the received polarization p (v_s or h_s) and the transmitted polarization q (v or h), the scattered polarization and depolarized fields are obtained [23, 50] from

$$
\begin{aligned}
\mathbf{E}^s_{pq} &= (\mathbf{v}'_s.\mathbf{p})\{(\mathbf{q}.\mathbf{v}')S_{v'_s v'} + (\mathbf{q}.\mathbf{h}')S_{v'_s h'}\}E_0 \\
&\quad +(\mathbf{h}'_s.\mathbf{p})\{(\mathbf{q}.\mathbf{v}')S_{h'_s v'} + (\mathbf{q}.\mathbf{h}')S_{h'_s h'}\}E_0
\end{aligned} \tag{8}
$$

Then the average $\left\langle E^s_{pq} E^{s*}_{p'q'} \right\rangle$ with respect to the large-scale roughness can be calculated and rewritten in terms of the scattering coefficients σ^s_{pq} [23–25, 50] as a function of the transmitter polarization q and the receiver polarization p. From the previous mathematical developments we notice that TSM is based on the SPM approach adapted to intermediate and grazing angles by the tilting process.

However the here presented TSM is not adapted to evaluate the specular component. Actually, the approach applied in the present paper is a composite TSM. The specular component evaluated using the KA is added to the TSM evaluation [50]. Nevertheless, for the sake of simplicity, this composite TSM approach is only called TSM in the following.

Finally, it worth to highlight the fact that the TSM has a wider application domain than the KA and the SPM approaches. It covers the small and the large waves. In other word our composite bistatic TSM approach is very well adapted to estimate the specular electromagnetic fields as well as intermediate and grazing ones.

4 SCATTERING MATRIX SIMULATION

In the previous sections, we presented a brief outline of different models for electromagnetic scattering (KA, SPM, SSA, CMOD, TSM) and sea roughness (Cox-Munk probability density function, Pierson-Moskowitz and Elfouhaily spectra). The main purpose of our study consists in the comparison of these various approaches. More precisely, our numerical study underlines the influence of these different theoretical models in a bistatic configuration.

Although the bistatic configuration is our main subject, the first part of this numerical section is dedicated to the backscattering configuration in order to compare our results with the already published theoretical studies and experimental data.

It is noteworthy that in a backscattering or in any forward-backward configuration the cross-polarization components only represent the depolarization effect of the sea surface. Using the classical models (KA,SPM), this phenomenon is not taken into account and the cross polarization coefficients are assumed to be null. Astonishingly, due to the local tilting processes, the cross polarization coefficients estimated with the TSM are non zero terms. The validity of these coefficients in backscattering or in forward-backward configurations is not investigated in the present study, nevertheless the cross polarisation components are also presented in our numerical simulations. Anyway, it is important to notice that in any other bistatic configuration the cross-polarization coefficients mainly represent a geometric rotation between the incident and the scattered frames of reference. In these cases, the validity of the TSM approach is absolutely justified.

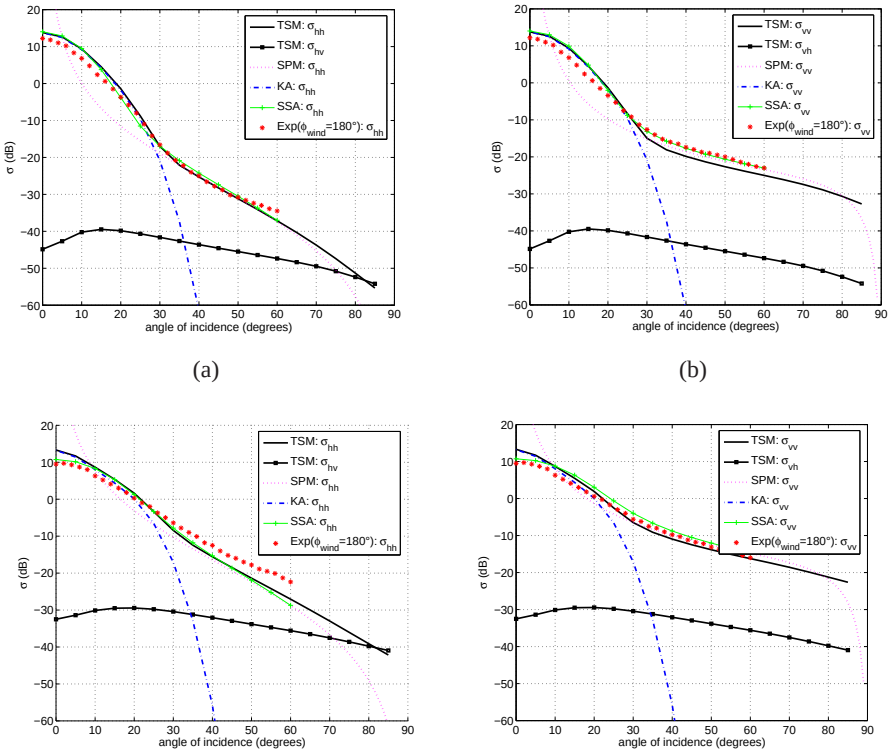

Fig. 5. Backscattering coefficients with different models F=14GHz, $T = 20°C$, S=35ppt, wind speed=5m/s (a, b) and 15m/s (c, d) (at 10 meters)(TSM ($\sigma_{h_s h}$, $\sigma_{h_s v}$ (a,c), $\sigma_{v_s v}$, $\sigma_{v_s h}$ (b,d)), SPM ($\sigma_{h_s h}$ (a,c), $\sigma_{v_s v}$ (b,d)), KA ($\sigma_{h_s h}$ (a,c), $\sigma_{v_s v}$ (b,d)), SSA ($\sigma_{h_s h}$ (a,c), $\sigma_{v_s v}$ (b,d)) are compared with Voronovich experimental data [18])

4.1 Backscattering Configuration

The backscattering configuration is obviously of utter importance in many applications as classic radars, satellite SAR images [59] and others electromagnetic sensor systems. Therefore, the numerical results in scientific references are almost solely given for backscattering problems. That is the reason why at first we present our numerical evaluations in this context.

Thus the backscattering configuration involves that incident emission and reception directions must be the same and the corresponding azimuth difference equal to π. If we refer to figure 3, we must assume the following relations:

$$\theta = \theta_s \qquad and \qquad \phi_s = \phi + \pi \tag{9}$$

The first simulation, see (figure 5), deals with the incidence angle effect on the scattering coefficients. The electromagnetic frequency is fixed to 14 GHz (K_u Band), the scale-dividing parameter k_d (for the two-scale model) is set to one third of the emission wave number ($k_d = \frac{k}{3}$), the wind speed to 5 m/s then to 15 m/s at a 10 meters altitude above the sea surface and the emitter is supposed to be in the downwind direction. More, the TSM and the SPM are evaluated using the unified spectrum (Elfouhaily spectrum).

For KA and SPM only direct-polarization cross sections (σ_{hh} and σ_{vv}) are estimated. As the same way as previous studies [18], we compare the theoretically predicted backscattering cross sections at K_u-Band versus the empirical SASS-II model, based on three months of Seasat

measurements [60, 61]. The SASS-II model was also confirmed by comparisons with airborne measurements [62, 63]. In examining the data points [18] used in (fig-5), several items of importance may be deduced from the graphs. First, there is a rather good agreement between the calculated cross sections and the ocean measurements depending on the used approach and sea representation. Near the normal (specular region in backscattering configuration $\theta = \theta_s \in [0°, 20°]$) KA is really fitted to the data. This observation appears as logic since the KA hypotheses are fulfilled in this configuration.

In the median region ($\theta = \theta_s \in [25°, 60°]$) SPM, as well as the TSM and the SSA are the adequate approaches for this domain. In this case waves are relatively small compared to the spatial wave number. For the grazing angles ($\theta = \theta_s > 60°$) neither the KA nor the SPM are adapted to determine the scattering matrix coefficients. However the TSM approach gives credible results. Indeed when focusing in the local reference frame we can use SPM since we respect its hypothesis, the averaging result by the slope distribution (tilting process) will adapt the results to the global reference.

If we compare the TSM with the SSA approach, we can notice that the difference is not really significant. Nevertheless, it must be underlined that, for large incident angles (above $60°$), SSA raises great numerical problems and does not provide reliable results. Futhermore, contrary to TSM, cross polarization is not yet modeled using SSA.

This simulation shades light on the influence of wind upon the electromagnetic sea surface scattering. As wind velocity decreases, the electromagnetic scattered field goes primarily in the specular direction (the normal direction in the backscattering configuration). In the opposite case, the increase of the wind velocity involves that the electromagnetic amplitude is significantly attenuated (several dBs).

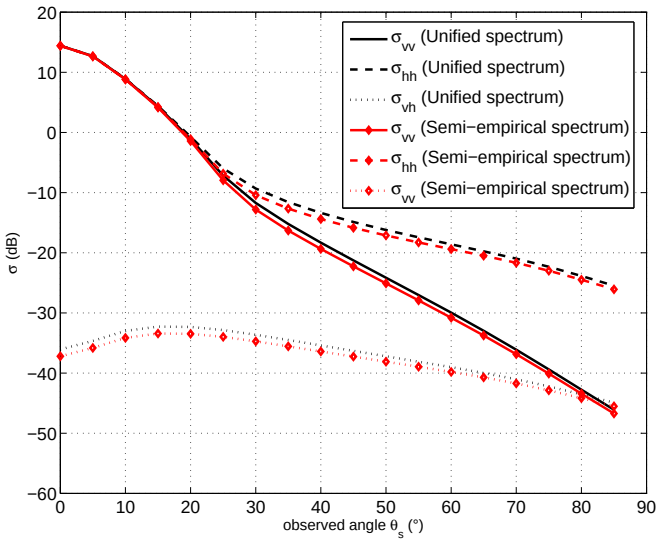

Fig. 6. Backscattering coefficients using different sea spectra (F=14 GHz, $T = 20°C$, S=35ppt, wind speed=15 m/s (at 10 m))

Besides, from the graph (figure 6) we may evaluate the impact of the various sea surface representations (sea spectra) through the backscattering coefficients. The results point out a difference of 0 to 2 (dB) between the Unified spectrum and the semi-empirical spectrum, for any coefficients.

In the next graph (figure 7) we analyze the wind direction influence upon the sea surface scattering. The incident angle is then fixed to $40°$ and we vary the azimuth relative to upwind

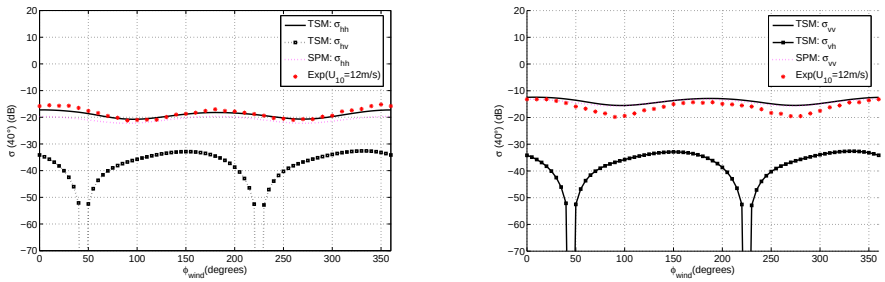

(a) (b)

Fig. 7. Wind direction effect on backscattering coefficients F=14 GHz, $T = 20°C$, S=35ppt, wind speed=12 m/s (at 10 m), θ=θ_s=40°) (TSM ($\sigma_{h_s h}$, $\sigma_{h_s v}$ (a), $\sigma_{v_s v}$, $\sigma_{v_s h}$ (b)), SPM ($\sigma_{h_s h}$ (a), $\sigma_{v_s v}$ (b)), KA ($\sigma_{h_s h}$ (a), $\sigma_{v_s v}$ (b)) are compared with [39] experimental data

speed from $0°$ to $360°$. Simulations were computed for a wind speed of 12 m/s and for an altitude of 10 meters above the sea surface. Results are compared with data presented by [39].

Figure 7 reveals that electromagnetic coefficients reach their maximum for both the upwind and downwind directions and their minimum at the cross wind directions. TSM and SPM confirmed their validity for the intermediate domain since results are in good agreement with Moore et al. [39] data for an incidence angle of $40°$. The Kirchhoff approach is not exploitable in this case since we are far from the specular region.

In figure 8 we deduce the velocity wind influence on the electromagnetic scattering by the sea surface for different incident angles: near specular ($\theta = 20°$), intermediate ($\theta = 40°$) and in the grazing angles zone ($\theta = 80°$). Simulations are compared with CMOD-IFR2 data published by Lemaire et al. [64].

TSM results are in a good accordance with CMOD measurements specially for the intermediate angles ($\theta = 60°$) and both sea spectra show a good agreement for all application domain.

In the next section, different configurations will be treated in order to compare the electromagnetic scattering models using the unified spectrum.

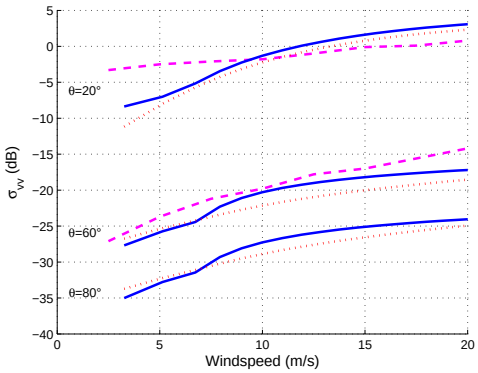

Fig. 8. Wind velocity effect on backscattering coefficients for F=6.5 GHz, $T = 20°C$, S=35ppt and wind azimuth $\phi_{wind} = 135°$. The continuous, the dotted and dashed lines represent respectively the TSM using the unified spectrum, The TSM using the semi-empirical spectrum and the CMOD-IFR2 model [64]

4.2 Forward-Backward Configuration

In this configuration, we set the emitter incident angle to $60°$ then to $80°$. The emitter azimuth is $0°$, wind relative azimuth is $0°$ (upwind), the electromagnetic wave frequency is 14 GHz (K_u Band), receiver azimuth is $180°$ and we let the receiver incident angle θ_s vary from $-90°$ to $90°$. This configuration enables the evaluation of both the specular and the diffuse components.

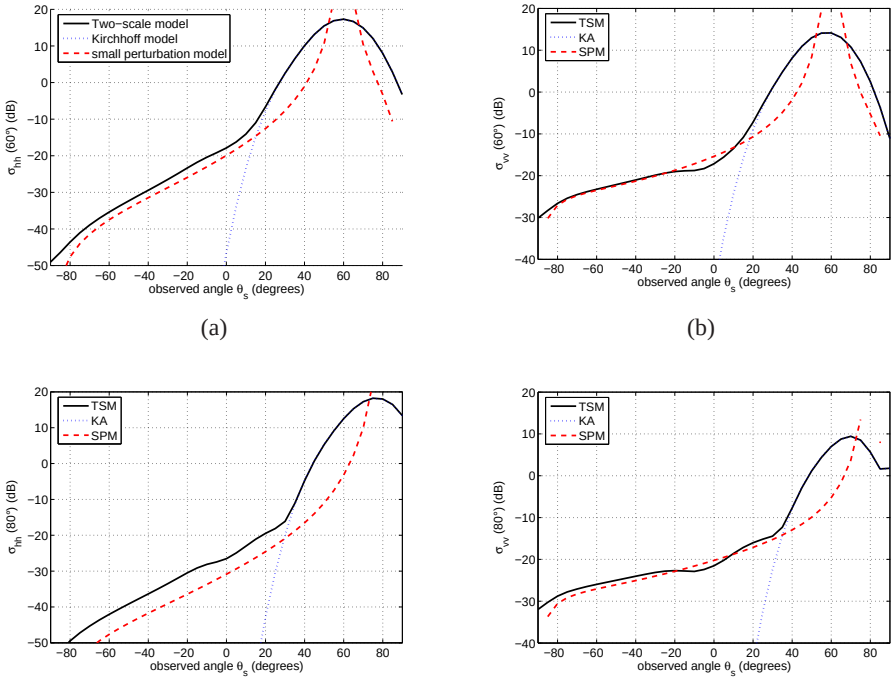

Fig. 9. Scattering coefficients (forward-backward configuration) F=14 GHz, T=20°C, S=35ppt, wind speed=5 m/s (at 10 m) ϕ_s=180°, θ=60° (a,b) and θ=80° (c,d))

Figure 9 confirms the limits of the two classical approaches and the supremacy of the two-scale model. This later cover specular, intermediate and the grazing regions. For any polarization coefficient, the TSM and the KA correspond to the same estimation in the specular direction area (more or less $20°$). This remark illustrates the fact that our TSM approach is actually a composite TSM. For vertical polarization, the TSM is almost similar to the SPM outside the specular lobe. For horizontal polarization, this statement is only valid if the incident angle is not too large. For θ=80°, the SPM curve is about 5dB lower than the TSM one.

From a general point of view, the forward-backward configuration is a particular case of the bistatic configuration [65]. We fix the emitter and let the position of the receiver vary in the emitter plane. In the next paragraph we present the general bistatic configurations [24, 66] for different emitter and receiver positions.

4.3 Bistatic Configuration

In this section, in order to provide a global view of the sea surface electromagnetic scattering, we set the emitter angles to θ=60° and ϕ=0° and we vary the receiver position, where $\theta_s \in [0°, 90°]$ and $\phi_s \in [0°, 360°]$.

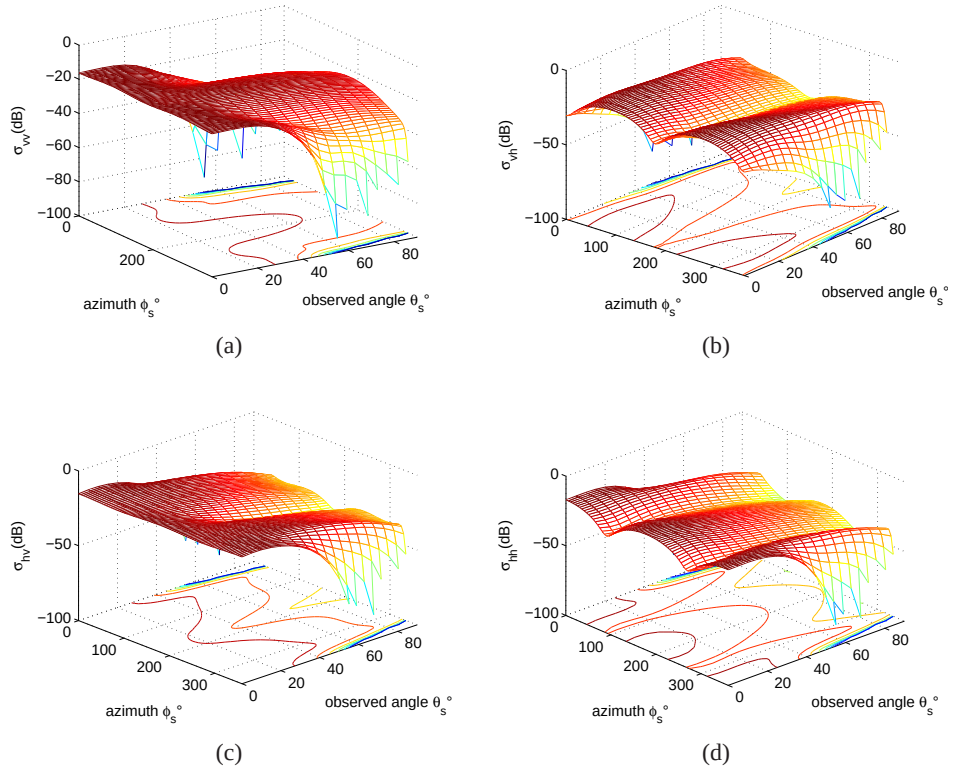

Fig. 10. Scattering coefficients (bistatic configuration) F=14 GHz, $T = 20°C$, S=35ppt, wind speed=15 m/s (at 10 m) ϕ=0° and θ=60°

From (fig-10) one notes that in vv and hh polarizations, the scattered signal energy is mainly located in the specular region. On the opposite, cross polarized coefficients reach a minimum in the plane of specular propagation (ϕ_s=0° or ϕ_s=180°). In this plane, the cross polarization is only due to the depolarization by the sea surface and this phenomenon provides a quite weak component. As previously said, in any other bistatic configuration, the cross polarization is mainly due to the rotation between the incident and the scattered frames of reference.

To illustrate this statement, we can consider the case where the receiver azimuth is set to $90°$ (figure 11). In this simulation, we determine a bistatic configuration where the emitter incident angle is fixed respectively to $40°$ and $60°$, the incident azimuth to $0°$, relative wind azimuth to $0°$ (upwind), electromagnetic frequency to 14 GHz (K_u Band) and we let the observed angle of the receiver θ_s vary from $-90°$ to $90°$. Only the two-scale approach is investigated here.

In figure 11, we can notice that the cross polarired coefficients dominate the direct polarised ones for θ near zero. As a matter of fact, for $\theta = 0$, a horizontal component in the incident frame of reference corresponds to a vertical one in the scattered frame of reference. In this case the cross polarized component is not related to any depolarization phenomenon.

In any case, a very important point is that the use of various bistatic configurations can be a great source of information for remote sensing application. For instance, the observation of the

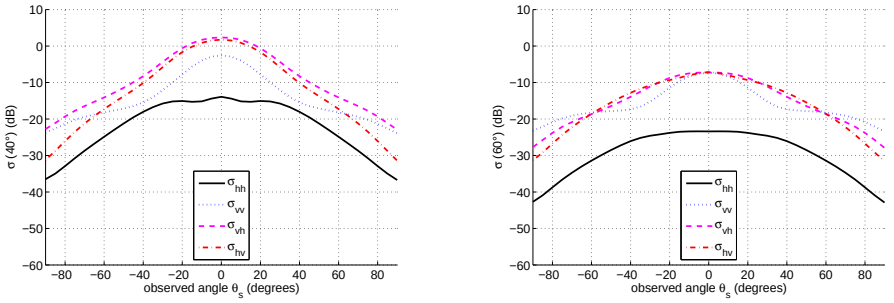

(a) (b)

Fig. 11. Scattering coefficients (bistatic configuration) F=14 GHz, $T = 20°C$, S=35ppt, wind speed=15 m/s (at 10 m) ϕ_s=90°, θ=40° (a) and θ=60° (b)

wind direction using electromagnetic sensors in bistatic or in forward-backward configuration remains a quite difficult task. In figure 12, we consider the case where $\theta = \theta_s = 45°$ and where the receiver azimuth ϕ_s vary from 0 (specular direction) to $180°$ (backscattering direction). These simulation are done with different wind directions ($0°$, $20°$, $40°$, $60°$, $90°$).

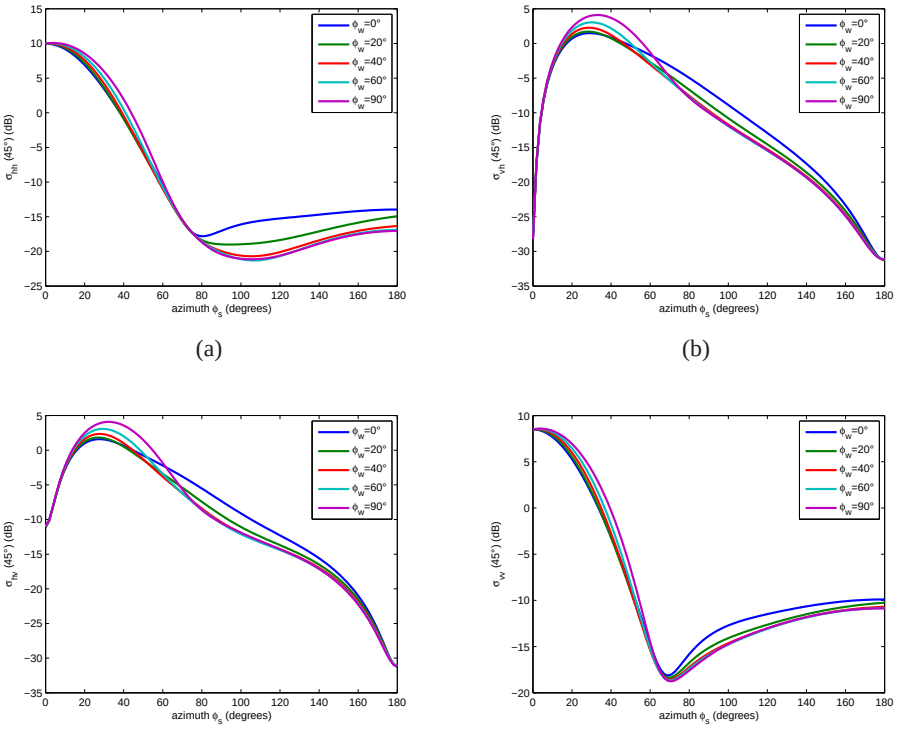

(a) (b)

(c) (d)

Fig. 12. Scattering coefficients (bistatic configuration) F=14 GHz, $T = 20°C$, S=35ppt, wind speed=15 m/s (at 10 m) θ_s=45° and θ=45°

It clearly appears that the specular and the backscattering directions are not the most relevant to study the influence of the wind direction. In other respects, we note that the curves corresponding to the direct polarized coefficients have a minimum between $\phi_s = 0$ and $\phi_s = 180°$.

It worths to notice that, for vertical polarization, the position of the minimum does not seem to be influenced by the wind direction. On the contrary, the position of the minimum related to the horizontal component is modified by the wind direction. This example highlights the importance of the bistatic configurations to identify properties of the sea surface.

5 ELECTROMAGNETIC SIGNAL SIMULATION

In this section, we simulate, as an illustration of the bistatic configuration, the received signal scattered by the sea surface when the incident wave is plane. In these conditions, the simulation consists to add the contribution of each elementary sea surface. Each elementary contribution is determined using the bistatic scattering matrix. Furthermore, the sea surface is supposed to be incoherent and the sum of energy is considered.

Nevertheless, this sum must take into account the delay related to each ray (elementary contribution). Therefore, we must add the contributions with the same delay. In the present case, these contributions correspond to sea surfaces in the area limited by intersection of two Fresnel ellipsoids, see figure (13(a)).

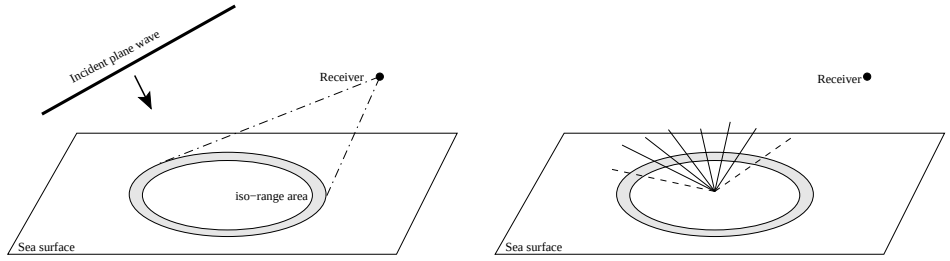

(a) Isorange area (b) Angular section

Fig. 13. Elementary area

Then, these annular zones, between two iso-range lines, are divided into a great number of angular sectors to obtain elementary surfaces, see figure (13(b)).

As an example, the carrier wave is the assumed to be circularly polarized. To compute the scattering coefficients using the TSM approach, the received signal is split into two linearly polarized waves (horizontal and vertical components). Moreover, the angle of incidence is set to $45°$, the receiver is at 50 meters above the sea and the frequency of the incident signal is in L-band ($1.5\,GHz$).

These simulations highlight the influence of the sea conditions upon the reception of scattered signals in a maritime environment. The figure (14) illustrates the modification of the power density distribution (impulse response) when the weather conditions change. For a quite low coefficient on the Beaufort scale, the scattering by the sea surface can be reduced to a quasi specular reflection. But, when the coefficient is higher, the diffuse component is important and the average delay of the scattered signals grows.

6 CONCLUSION

In this paper, the numerical simulation of the electromagnetic scattering by ocean surfaces is described, based on TSM approach and realistic description of the sea. The comparison with large amounts of previously published results is carried out. Moreover, the originality of our study lies in the bistatic configurations that are hardly ever presented.

Not only our numerical results are consistent with measured data, with a semi-empirical model (CMOD5) and with other analytical models (Small Slope Approximation) in backscattering configurations, but we also present cross-polarization, non-standard bistatic and large incident angle (near grazing) configurations.

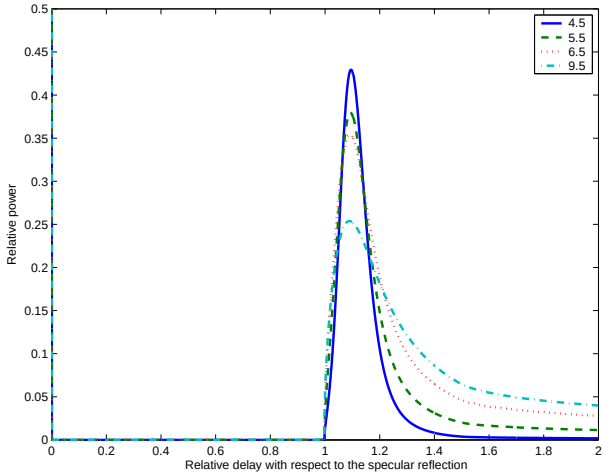

Fig. 14. Numerical simulation of the signal power (impulse response) received above sea surface (with different Beaufort wind scale coefficients: 4.5,5.5,6.5 and 9.5)

Finally, we show that our approach can be usefully applied to simulate the signal received by an observer above the sea when a plane incident wave impinges on the ocean surface.

APPENDIX A: COX & MUNK SLOPE PROBABILITY DENSITY FUNCTION

As previously seen in section 2, the slope distributions are one of the most common approaches used to describe the ocean roughness. The key point is then to determine the slope probability density function.

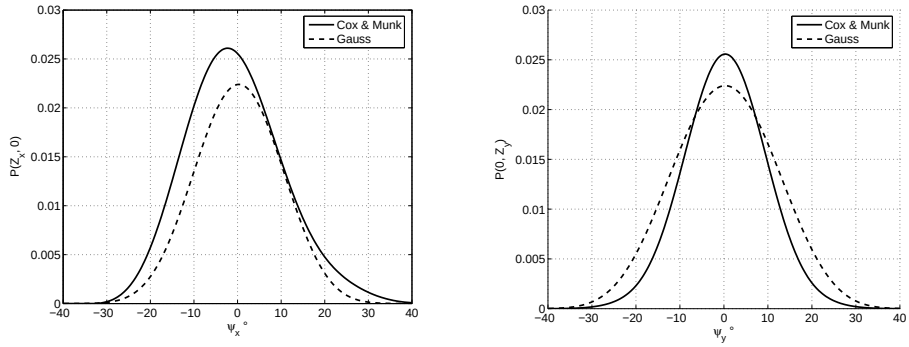

(a) Upwind (b) Crosswind

Fig. 15. Slope distribution representation (wind speed $U_{12.5} = 15m/s$ and $\psi_x = \arctan(Z_x)$)

The first form used in the literature to define sea slope probability density function was the Gaussian expression [10,44,45]. As represented in figures 15(a) and 15(b), we note the function symmetry in the upwind direction. According to [26], actual data show that there is some up/downwind skewness which increases with the wind speed. As a result the most probable slope at high winds is not zero, with the azimuth of ascent pointing downwind. Contrary to the Gaussian distributions, the Cox & Munk probability density function is not centered and illustrates this skewness phenomenon.

References

[1] L. M. Brekhovskikh, "The diffraction of waves by a rough surface, part I and II," *Zh. Eksper. i Teor. Fiz* **23**, 275–304 (1952).

[2] A. K. Fung, W. Y. Liu, and K. S. Chen, "A comparison between IEM-based surface bistatic scattering models," in *IEEE Int. Geosci. Rem. Sens. Symp.*, **02**(1), 441–443 (2002) [doi:10.1109/IGARSS.2002.1025066].

[3] A. K. Fung, *Microwave Scattering and Emission Models and their Applications*, Artech House (1994).

[4] G. R. Valenzuela, "Depolarisation of EM waves by slightly rough surfaces," *IEEE Trans. Antennas Propagat.* **AP-15**(4), 552–557 (1967) [doi:10.1109/TAP.1967.1138962].

[5] S. O. Rice, "Reflection of electromagnetic waves from slightly rough surfaces," *Commun. Pure. Appl. Math* **4**, 351–378 (1951) [doi:10.1002/cpa.3160040206].

[6] L. Rayleigh, *The theory of sound*, vol. 2, dover, New York (1945).

[7] F. T. Ulaby, R. K. Moore, and A. K. Fung, *Microwave Remote Sensing: Active and Passive*, vol. 2, Artech House Publishers (1982).

[8] A. Ishimaru, *Wave propagtion and scattering in random media*, vol. **1,2**, Academic Press, Inc (1978).

[9] F. T. Ulaby and C. Elachi, *Radar polarimetry for geoscience application*, Artech house, Bostan MA (1990).

[10] A. K. Fung, Z. Li, and K. S. Chen, "Backscattering from a randomly rough dielectric surface," *IEEE Trans. Geosci. Rem. Sens.* **30**, 356–369 (1992) [doi:10.1109/36.134085].

[11] A. K. Fung, Z. Li, and K. S. Chen, "An improved model for bistatic scattering from rough surfaces," *J. Electromag. Waves Appl.* **30**, 356–369 (1992).

[12] M. Licheri, N. Floury, M. Borgeaud, and M. Migliaccio, "On the scattering from natural surfaces: the IEM and the improved IEM," in *IEEE Int. Geosci. Rem. Sens. Symp.*, **01**, 2911 – 2913, (Sydney, Australia) (2001) [doi:10.1109/IGARSS.2001.978203].

[13] M. Marrazzo, R. Sabia, and M. Migliaccio, "IEM sea surface scattering and the generalized p-power spectrum," in *IEEE Int. Geosci. Rem. Sens. Symp.*, **03**(1), 136–138 (2003).

[14] F. Koudogbo and P. F. Combes, "Numerical and experimental validations of IEM for bistatic scattering from natural and manmade rough surfaces," *Prog. Electromag. Res.* **46**, 203–244 (2004) [doi:10.2528/PIER03092902].

[15] A. G. Voronovich, "Small-Slope Approximation in wave scattering by rough surfaces," *Sov. Phys. JETP* **62**, 65–70 (1985).

[16] A. G. Voronovich, "Small-Slope Approximation for electromagnetic wave scattering at a rough interface of two dielectric half-spaces," *Waves Random Media* **4**, 337–367 (1994) [doi:10.1088/0959-7174/9/4/304].

[17] A. G. Voronovich, *Wave scattering from rough surfaces*, Springer (1998).

[18] A. G. Voronovich and V. U. Zavorotny, "Theoretical model for scattering of radar signals in Ku- and C-bands from a rough sea surface with breaking waves," *Waves Random Media* **11**, 247–269 (2001) [doi:10.1088/0959-7174/11/3/305].

[19] S. A. Boukabara, L. Eymard, C. Guillou, D. Lemaire, P. Sobieski, and A. Guissard, "Development of a modified two scale electromagnetic model simulating both active and passive micorwave measurments: comparison to data remotely sensed over the ocean," *Radio Sci.* **37**(4), 161–1611 (2002) [doi:10.1029/1999 RS002240].

[20] A. Guissard and P. Sobieski, "An approximate model for the microwave brightness temperature of the sea," *Int. J. Rem. Sensing* **8**(11), 1607–1627 (1987).

[21] E. Obligis, "In-fight calibration/validation of the ENVISAT/MWR," *Tech. Rep. of* WP3000, ESA Contract No. 13681/99/NL/GD (2001).

[22] J. Boutin, E. Obligis, and E. Dinnat, "Influence of surface roughness on Tb simulated in L-band by Yueh-LODYC emissivity model and by UCL model - analyse of the differences," *Tech. Rep.* 14273/00/NL/DC, ESTEC/European Space Agency (2002).

[23] A. Khenchaf and O. Airiau, "Bistatic radar moving returns from sea surface," *IEICE Trans. Elect.* **E83**, 1827–1835 (2000).

[24] A. Khenchaf, "Scattering and propagation above any random rough surface at near-grazing angles," *RTO-MP*-**60** , 32–1 32–7 (2000).

[25] A. Khenchaf, F. Daout, and J. Saillard, "The two-scale model for random rough surface scattering," in *Prospects for the 21st Century, IEEE Proc. Oceans*, **96**, 50–54 (1996) [doi:10.1109/OCEANS.1996.568346].

[26] C. Cox and W. Munk, "Statistics of the sea surface derived from sun glitter," *J. Mar. Res.* **13**, 198–226 (1954).

[27] C. Cox and W. Munk, "Slopes of the sea surface deduced from photographs of sun glitter," *Bull. Scripps. Inst. of Oceanog.* **6**, 401–488 (1956).

[28] W. J. Pierson and L. Moskowitz, "A proposed spectral form for fully developped wind sea based on the similarity theory of S. A. Kitaigorodskii," *J. Geophys. Res.* **69**, 5181–5190 (1964).

[29] O. M. Phillips, *The dynamics of the upper ocean*, Cambridge university press (1966).

[30] G. Neumann and W. J. Pierson, *Principles of physical oceanography*, Prentice-Hall, Englewoods cliffs (1966).

[31] K. Hasselmann, *Measurment of wind-wave growth and swell during the joint north sea project (JONSWAP)*, vol. **12**(95), Dtsch. Hydrogr. Z. (1973).

[32] M. A. Donlean and W. J. Pierson, "Radar scattering and equilibrium ranges in wind-generated waves with application to scattometry," *J. Geophys. Res.* **92**, 4971–5029 (1987).

[33] T. Elfouhaily, B. Chapron, and K. Katsaros, "A unified directional spectrum for long and short wind-driven waves," *J. Geophys. Res.* **102**, 15,781–15,796 (1997) [doi:10.1029/97JC00467].

[34] C. Cox and W. Munk, "Measurment of the roughness of the sea surface from photographs of the sun's glitter," *J. Opt. Soc. Am.* **44**, 838–850 (1954).

[35] A. K. Fung and K. K. Lee, "A semi-empirical sea-spectrum model for scattering coefficient estimation," *IEEE J. Oceanic Engin.* **OE-7**(4), 166–176 (1982) [doi:10.1109/JOE.1982.1145535].

[36] J. W. Wright, "A new model for sea clutter," *IEEE Trans. Antennas Propagat.* **AP-16**(2), 217–223 (1968).

[37] G. R. Valenzuela, "Theories for the interaction of electromagnetic and oceanic waves- a review," *Boundary-Layer Meteorology* **13**, 61–85 (1978) [doi:10.1007/BF00913863].

[38] C. Elachi and W. E. Brown, "Models of radar imaging of the ocean surface waves," *IEEE Trans. Antennas Propagat.* **AP-25**(1), 84–94 (1977).

[39] R. K. Moore, A. K. Fung, G. J. Dome, and I. J. Birrer, "Estimates of oceanic surface wind speed and direction using orthogonal beam scatterometer measurments and comparaison of recent sea scattering theories," Tech. Rep. 186-17 also NASA Contractor Rep. 158908, University of Kansas Remote Sensing, NASA Langley Res. Ctr. Hampton, VA (1978).

[40] A. Mouche, D. Hauser, J.-F. Daloze, and C. Guérin, "Dual-polarization measurements at C-band over the ocean: Results from airborne radar observations and comparison with envisat asar data," *IEEE Trans. Geosci. Rem. Sens.* **43**(4), 753–769 (2005) [doi:10.1109/TGRS.2005.843951].

[41] D. E. Barrick, "Rough surface scattering based on the specular point theory," *IEEE Trans. Antennas Propagat.* **AP-16**(4), 449–454 (1968).

[42] D. E. Barrick and E. Bahar, "Rough surface scattering using specular point theory," *IEEE Trans. Antennas Propagat.* **AP-29**(5), 798–800 (1981).

[43] D. E. Barrick and R. Fitzgerald, “The failure of ”classic” perturbation theory at a rough neumann boundary near grazing,” *IEEE Trans. Antennas Propagat.* **48**(9), 1452–1460 (2000) [doi:10.1109/8.898780].

[44] G. S. Brown, “Backscattering from a Gaussian-distributed perfectly conducting rough surface,” *IEEE Trans. Antennas Propagat.* **AP-26**(3), 472–482 (1978) [doi:10.1109/TAP.1978.1141854].

[45] K. Sarabandi, Y. Oh, and F. T. Ulaby, “A numerical simulation of scattering from one-dimensional inhomogeneous dielectric random surfaces,” *IEEE Trans. Geosci. Rem. Sens.* **34**, 425–432 (1996) [doi:10.1109/36.485120].

[46] W. J. Pierson, “The theory and applications of ocean wave measuring systems at and below the sea surface, on land, from aircraft and from spacecraft,” NASA *contract report* CR-2646n, NASA (1976).

[47] H. L. Chan and A. K. Fung, “A theory of sea scatter at large incident angles,” *J. Geophys. Res.* **82**, 3439–3444 (1977).

[48] A. Guissard, “Directional spectrum of the sea surface and wind scatterometry,” *Int. J. Rem. Sensing* **14**(8), 1615–1633 (1993) [doi:10.1080/01431169308953989].

[49] J. A. Oglivy, *Theory of wave scattering from random rough surfaces*, Bristol: Adam Hilger (1991).

[50] A. Khenchaf, “Bistatic scattering and depolarization by randomly rough surface: application to the natural rough surface in X-band,” *Waves Random Media* **11**, 61–87 (2001) [doi:10.1088/0959-7174/11/2/301].

[51] F. W. Millet and K. F. Warnick, “Validity of rough surface backscattering models,” *Waves Random Media* **14**, 327–347 (2004) [doi:10.1088/0959-7174/14/3/008].

[52] T. M. Elfouhaily and C. A. Guerin, “A critical survey of approximate scattering wave theories from random rough surfaces,” *Waves Random Media* **14**, R1–R40 (2004) [doi:10.1088/0959-7174/14/4/R01].

[53] P. Beckmann, *The depolarization of electromagnetic waves*, The golem press, Boulder Colorado (1968).

[54] A. Awada, A. Khenchaf, A. Coatanhay, and M. Y. Ayari, “Comparaison between small slope approximation and two scale model in bistatic configuration,” in *IEEE Int. Geosci. Rem. Sens. Symp.*, **05** (2005) [doi:10.1109/IGARSS.2005.1525369].

[55] A. Awada, A. Khenchaf, A. Coatanhay, and M. Y. Ayari, “Small slope approximation and two scale model in bistatic configuration, application to the sea surface,” in *ECPS*, **05** (2005).

[56] M. L. Banner, “Equilibrium spectra of wind waves,” *J. Phys. Oceanogr.* **20**, 966–984 (1990) [doi:10.1175/1520-0485(1990)020¡0966:ESOWW¿2.0.CO;2].

[57] S. D. Haan and A. Stoffelen, *CMOD5*, *SAF/OSI/KNMI/TEC/TN/140* (2001).

[58] F. Bass and I. Fuks, *Wave Scattering from Statistically Rough Surfaces*, Pergamon, Oxford (1979).

[59] G. Franceschetti, M. Migliaccio, and D. Ricco, “On ocean SAR raw signal simulation,” *IEEE Trans. Geosci. Rem. Sens.* **36**(1), 84–100 (1998) [doi:10.1109/36655320].

[60] A. Bentamy, P. Queffeulou, Y. Quilfen, and K. Katsaros, “Ocean surface wind fields estimated from satellite active and passive microwave instruments,” *IEEE Trans. Geosci. Rem. Sens.* **37**, 2469–86 (1999) [doi:10.1109/36.789643].

[61] F. J. Wentz, S. Peteherich, and L. A. Thomas, “A model function for ocean radar cross section at 14.6GHz,” *J. Geophys. Res.* **89**, 3689–3704 (1984).

[62] J. R. Croswell, S. C. Carson, R. E. MacIntosh, F. K. Li, G. Neumann, D. J. McLaughlin, J. C. Wilkerson, P. G. Black, and S. V. Nghiem, “Airborne scatterometers: investigating ocean backscatter under low- and high-wind conditions,” *Proc. IEEE* **82**, 1835–60 (1994) [doi:10.1109/5.338074].

[63] W. J. Donnelly, J. R. Croswell, R. E. MacIntosh, P. S. Chang, J. Wilkerson, F. Marks, and P. G. Black, "Revised ocean backscatter model at C and Ku band under high-wind conditions," *J. Geophys. Res.* **104**(11), 485–97 (1999) [doi:10.1029/1998JC900030].

[64] D. Lemaire, P. Sobieski, and A. Guissard, "Full-range sea surface spectrum in nonfully developed state for scattering calculations," *IEEE Trans. Geosci. Rem. Sens.* **37**(2), 1504–1520 (1999) [doi:10.1109/36.752222].

[65] A. K. Fung, C. Zuffada, and C. Y. Hsieh, "Incoherent bistatic scattering from the sea surface at L-Band," *IEEE Trans. Geosci. Rem. Sens.* **39**, 1006–1012 (2001) [doi:10.1109/36.921418].

[66] A. Khenchaf, "The bistatic scattering from the natural rough surfaces in X and Ku bands," in *IEEE Int. Geosci. Rem. Sens. Symp.*, **01**, 2843–2845 (2001) [doi:10.1109/IGARSS.2001.978181].